# The Importance of XRD data to overcome the challenges of Clay Volume Estimation in K-Felspar and Kaolinite-rich unconsolidated reservoirs of the Paleocene age in the Tambaredjo Oil Field of Suriname

*Ferhaad* Idoe[1,*], *Arantxa* Lieveld[2**], *Elias* Acosta[1,], *Prachand* Naigi[3**], *Fabian* Graanoogst[1] and *Bhagwanpersad* Nandlal[4]

[1]Staatsolie Maatschappij Suriname N.V., Onshore Directorate, FSS - Formation Evaluation Department, Saramacca, Suriname
[2]Staatsolie Maatschappij Suriname N.V, Offshore Directorate, Deepwater Exploration contracted Acreage, Paramaribo, Suriname.
[3]Staatsolie Maatschappij Suriname N.V, Offshore Directorate, Appraisal Evaluation Team, Paramaribo, Suriname.
[4]Independant Consultant (former Functional Subsurface Support (FSS) Manager), Paramaribo, Suriname.
**former Onshore Directorate, FSS - Formation Evaluation Department.

**Abstract.** One critical aspect of formation evaluation revolves around the determination of clay volume (*Vcl*), as it significantly impacts the assessment of other petrophysical properties such as porosity ($\Phi$), water saturation (*Sw*), and permeability (*k*). Consequently, the accurate calculation of *Vcl* is imperative.

The indirect derivation of *Vcl* from logs and the direct measurement from cores are both vital methods. However, log-derived *Vcl* (*Log_Vcl*) methods may pose challenges in certain formations, leading to inaccuracies. In the Tambaredjo (TAM) field in Suriname, K-feldspar-rich intervals result in an overestimation of *Log_Vcl*, while kaolinitic intervals lead to an underestimation. The TAM field's oil-bearing reservoirs are in the reservoirs of Paleocene age, divided into 3 units namely the T3, T2, and T1 units based on depositional environment.

Following the inaccuracies, a comprehensive study was conducted involving data gathering, validation, expert assessments, and re-evaluation of *Log_Vcl* determination. The focus was on utilizing Core vs Log cross plots to identify distinct endpoints for the T3, T2, and T1 units, and separate endpoints for the K-feldspar-rich intervals. The proposed updated *Vcl* Model was developed based on the analyzed results.

Revising the endpoints resulted in the division of the T-unit into an upper (T3 Unit) and lower (T2 and T1 Unit) intervals. Utilizing unique endpoints for each unit significantly enhanced the reliability of the *Vcl* model, with a calibration difference of 1 to 5% between *Log_Vcl* and *XRD_Vcl*. It was recommended to use separate endpoints for K-feldspar-rich intervals, incorporating the use of Gamma ray Thorium for *Log_Vcl* calculations in such cases. Additionally, the Neutron-Density model or the Gamma ray method is suggested depending on the availability of Spectral Gamma ray and Neutron logs.

At present, the average between Larionov's Young Rocks and the Neutron-Density model is used for *Log_Vcl* calculations. This method presents a closer match with XRD data, addressing the underestimation and overestimation issues inherent in the individual approaches. Incorporating adjustments for the impact of K-feldspar and kaolinite further refines the *Log_Vcl* calculations. The proposed ultimate average approach assigns a 60% weight to Larionov's Young Rocks model and a 40% weight to the Neutron-Density model.

Re-evaluating the *Log_Vcl* can potentially yield a reduction of 5-10%, consequently leading to a 7-14% decrease in *Sw* and a more realistic estimation of Petroleum Initially In Place (PIIP). The outcomes of this project will also contribute to enhancing the *Vcl* model of the other onshore fields of Suriname.

## 1 Introduction

The precise determination of *Log_Vcl* is crucial for assessing reservoirs and estimating hydrocarbon reserves. A study in the TAM field sheds light on overcoming challenges in determining *Log_Vcl* in formations with varying mineralogies. The research emphasizes using unique endpoints for different T-Unit intervals and considering the impact of K-feldspar on *Log_Vcl.* The proposed *Vcl* model holds promise for similar fields. This study emphasizes the importance of accurately determining *Log_Vcl* for petrophysical reservoir evaluation and introduces a method for calibration with lab measurements and a new approach for *Vcl* calculation.

### 1.1 Area and Geological background.

Suriname, located in Northeastern South America, has three onshore oil fields that have been producing medium-heavy oil since 1982. These fields are operated by Staatsolie Maatschappij Suriname N.V in the Guiana Basin's Paleocene and Eocene reservoirs, with the largest field

being Tambaredjo (TAM), where oil is exclusively produced from the Paleocene reservoirs.

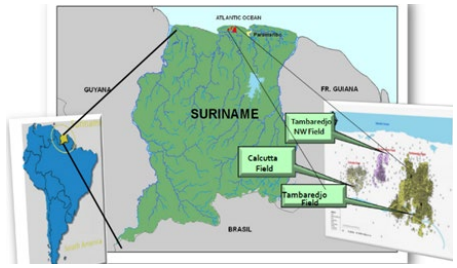


**Fig. 1.** Location map of the Staatsolie Onshore Oilfields [1].

The Paleocene T-Unit represents the foundational stratum of the Paleocene Saramacca Formation. It comprises a prograding fluvial sequence that encases the previously subaerial, weathered, and eroded surface of the underlying Cretaceous Nickerie Formation. The reservoir sands are overlain by a transgressive shale that onlaps onto the Cretaceous surface to the south. The T-Unit sands are further categorized into the lowermost T1, middle T2, and upper T3 sands based on the depositional environment. These sands are characterized by angular, medium to coarse-grained unconsolidated sands interbedded with clays. [2]

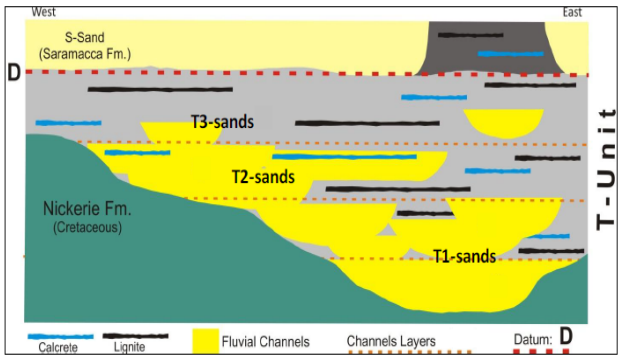


**Fig. 2.** The general stratigraphic model of the T-Unit, Saramacca Fm [2].

The X-ray diffraction (XRD) analysis conducted on cores extracted from the T-unit has indicated an overestimation in the estimation of *Log_Vcl*. Additionally, the XRD data has unveiled the presence of substantial quantities of K-feldspar in specific segments of the T-Unit. This geological setting has the potential to influence the *Log_Vcl*, subsequently impacting well-log interpretations and the accurate determination of clay volumes.

### 1.2 Previous Studies based on XRD data.

The calibration of *Log_Vcl* typically involves comparing them with core data, such as XRD data [3], which are known for their superior accuracy and precision compared to logging devices. This comparison serves as the basis for establishing the ground truth for other formation evaluation measurements. Therefore, it is crucial to calibrate the *Log_Vcl* using core data to validate the accuracy of the values obtained from the logs.

Fig 3 depicts an ideal scenario that can serve as a reference during the calibration process. The X-axis represents *XRD_Vcl,* while the Y-axis represents *Log_Vcl*. Ideally, *Vcl* should align closely with the 100% agreement line to ensure precise calibration.

Numerous studies have been undertaken over the years to enhance petrophysical parameters, particularly in *Log_Vcl* calculations. Torn [4] recommended the use of GRKT logs for VCLGR calculations, while Pan Terra GeoConsultants [5] proposed averaging VCLGR and VCLND to derive VCLAV as the final *Log_Vcl*, a method confirmed by Naigi's study in 2017 [6]. Liefeld [7] revealed that analyzing the formation through zoned endpoints yielded the most accurate *Log_Vcl*.

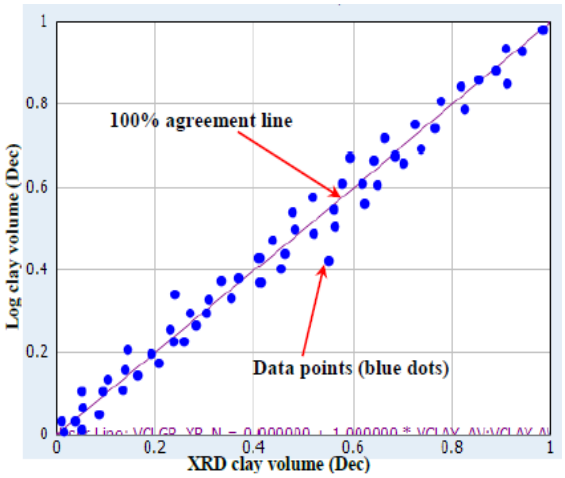


**Fig. 3.** XRD_$V_{cl}$ plotted against Log_$V_{cl}$, with a 100% agreement line representing the ideal situation [6].

### 1.3 Technical assessments.

The present approach to computing clay volume, which involves averaging VCLGR and VCLND, has been demonstrated to overstate clay content in certain formations. These overstatements result in inaccuracies in interpretations. For precise clay volume computations, a suitable calibration technique is imperative. Two Subject Matter Experts (SME), M. Deakin [8] and R. Aldred [9], assessed the current clay volume model and recommended the utilization of distinct endpoints for *Log_ Vcl* calculations. These unique endpoints can be acquired from Log data vs *XRD_Vcl* cross-plots. Log data supply insights into the subsurface formation, while XRD data provide information about the mineralogical composition of the rocks. Through the comparison of these two types of data, it is feasible to derive unique endpoints that can be consistently employed across various projects and reservoirs.

Furthermore, XRD analysis unveiled substantial concentrations of K-feldspar in specific segments of the T unit. Fig 4, track 3 demonstrates elevated GR readings for zone 2, indicating a high *Log_ Vcl*, while the N-D logs in track 4 signify a sandy formation over the same interval. XRD data plotted in track 5 verified that the formation is indeed sandy, and the VCLGR is overestimated. To prevent the inclusion of this K-feldspar content in the *Vcl*

computation, it was proposed to neutralize the impact of K-feldspar by employing the GR Thorium log (GR_THOR) as opposed to the GRKT log for *Log_ Vcl* determination.

The adoption of a more appropriate *Log_Vcl* calibration method, as proposed by the two experts, can significantly enhance the precision and uniformity of *Log_Vcl* estimations. This, in turn, can lead to more dependable reservoir characterization, improved decision-making, and enhanced PIIP.

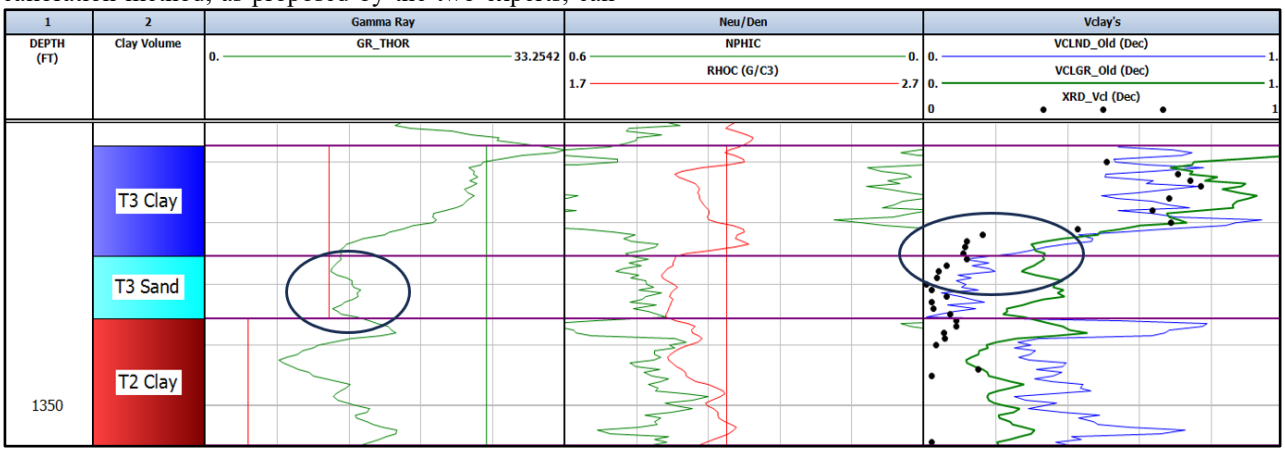


**Fig. 4.** Elevated Gamma Ray readings are leading to an overestimation of the volume of clay in the formation, while X-ray diffraction (XRD) and Neutron Density log (ND) data suggest a low clay volume within the same interval.

## 1.4 Current Vcl Calculation method

### *1.4.1 GR clay volume calculation model*

Currently, the $Log\_V_{cl}$ is calculated by using the following method:

The linear equation is used to calculate the Gamma Ray Index (GRI):

$$GRI = \frac{GR_{value\ (\log)} - GR_{clean}}{GR_{clay} - GR_{clean}} \qquad (1)$$

*Where: GRI = Gamma Ray Index; GR = Log GR (GAPI); GRClean = GRmin = GR in clean sand (GAPI); GRclay= GRmax = GR in clay/shale (GAPI)*

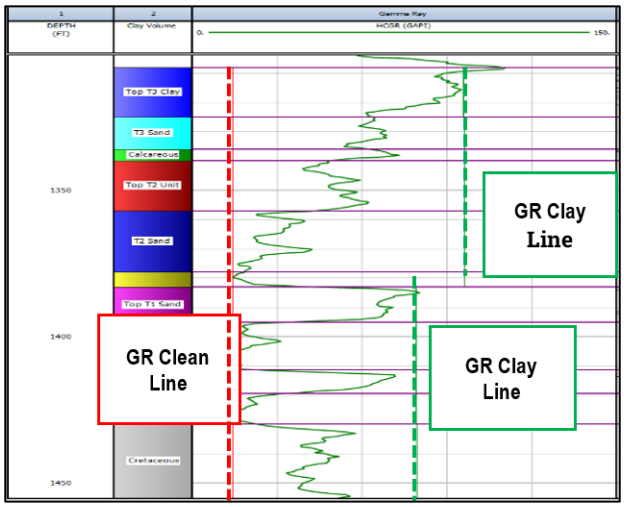


**Fig. 5.** GR log with GR Clean and GR Clay lines.

Given that the Paleocene age formations of the onshore fields from Staatsolie Maatschappij Suriname N.V. are unconsolidated, the Larionov (1969) Young Rock equation is employed for *Log_Vcl* calculations. The Young Rock relationship is utilized to deduce *Log_Vcl* from the GRI using the following equation:

$$Log\_Vcl = 0.083(2^{3.7IGR} - 1) \qquad (2)$$

The Larionov approach entails utilizing the GRKT curve, which is derived from SGR. In cases where spectral data is unavailable, the Gamma Ray (GR) is employed as an alternative. This approach is implemented separately for each zone, with each zone potentially having its own GR Clean and GR Clay parameters.

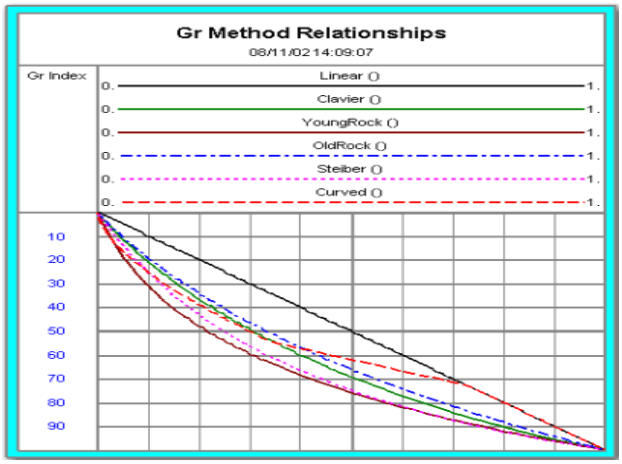


**Fig. 6.** Representation of equations GRI corrections [10].

### *1.4.2 Neutron-Density clay volume calculation model*

For the N-D *Vcl* method, the clay volume (VCLND) is determined using a combination of the Neutron (N) and Density (D) logs. The N-D clay volume model employs the principle of establishing a clean point and a clay point,

which are selected through interactive N-D cross plots. The calculation of *Vcl* is conducted using equation 3.

$$VCLND = \frac{((DenCl2 - DenCl1) \times (Neu - NeuCl1)) - ((Den - DenCl1) \times (NeuCl2 - NeuCl1))}{((DenCl2 - DenCl1) \times (NeuClay - NeuCl1)) - ((DenClay - DenCl1) \times (NeuCl2 - NeuCl1))} \quad (3)$$

*Where: DenCl1 & NeuCl1 and DenCl2 & NeuCl2 are the density and neutron values for the two ends of the clean line (IP 2023, help module)*

In accordance with the GRI endpoint selection criteria, distinct clean and clay points were ascertained for each well by utilizing N-D cross plots. Fig.7 illustrates an N-D cross plot depicting the determination of endpoints per zone.

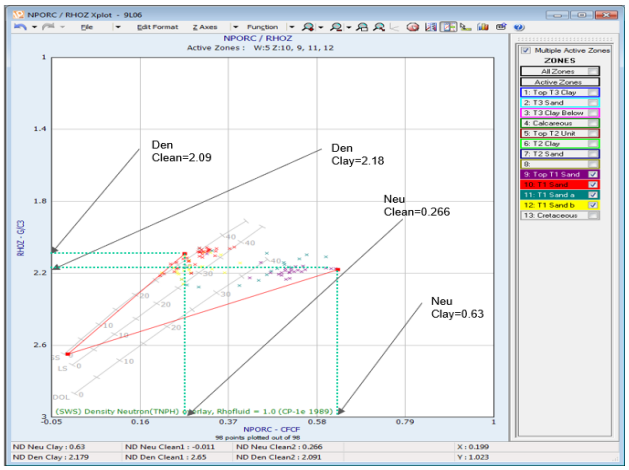


**Fig. 7.** N-D cross plot with Clean and Clay points for Neutron and Density.

As mentioned an average of the VCLGR and VCLND for calculations (VCLAV) is used.

Calculation of VCLAV:

$$VCLAV = \frac{(VCLGR + VCLND)}{2} \quad (4)$$

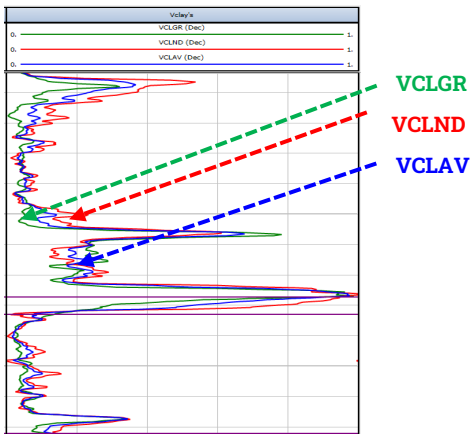


**Fig. 8.** Curves for VCLGR, VCLND, and VCLAV.

## 2 Methodology

### 2.1 XRD_Vcl vs Log_Vcl

To establish a reliable calibration, it is crucial to convert the *XRD Vcl* volume from dry clay volume (*Vdry_clay*) to wet clay volume (*Vwet_clay*). This is necessary because the *Log_Vcl* represents wet clay volume, while *XRD Vcl* represents dry clay volume. The conversion can be achieved by multiplying *Vdry_clay* with (1 - PHIT). Although there are numerous wells with XRD data in the TAM field, only the 4 wells systematically sampled over the T-unit were utilized for calibration. This selective approach ensures more dependable results. The four wells chosen for calibration are:

- 9L06
- 9B111
- 1M101
- 30HM111.

In Fig. 9, track 5, the disparity between *Vwet_clay* (black dots) and *Vdry_clay* (red dots) is visible for well 9L06.

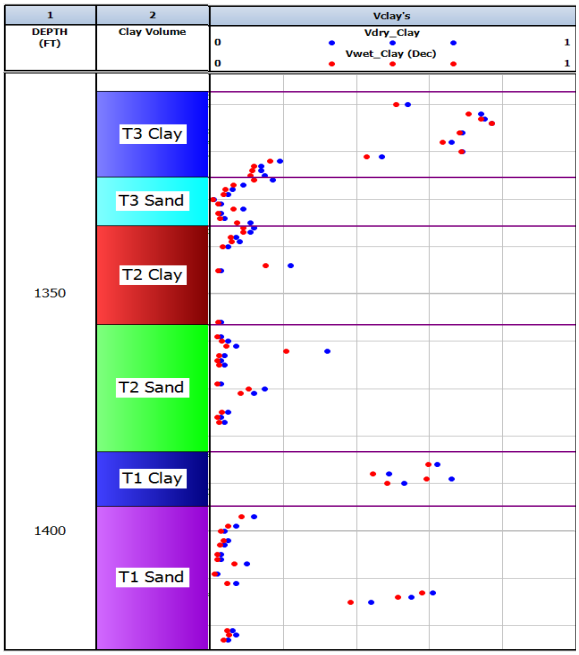


**Fig. 9.** Track 3 Indicates the differences between Vwet_clay (red dots) and Vdry_clay (blue dots).

### 2.2 Deriving unique endpoints from log to core calibrations.

To ensure the attainment of consistent endpoints, the parameters of GR, D and N were graphed against *XRD_Vcl*. The aim was to verify that the presence of K-felspar did not impact the *Log_Vcl* calculations, for which the GR_THOR curves were employed for calibration. As depicted in Figure 10, GR_THOR was plotted against *XRD_Vcl* to align the *Log_Vcl* with *XRD_Vcl.*

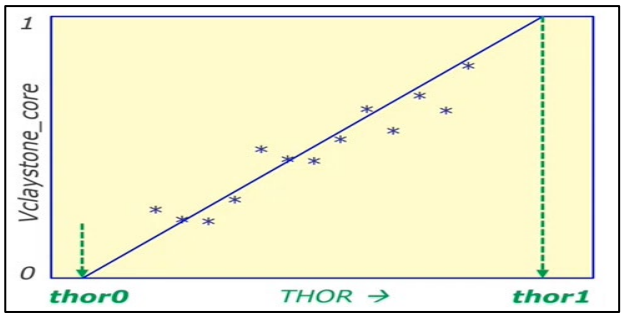


**Fig. 10.** Ideal representation of GR_THOR vs XRD_Vcl Cross plot for determining endpoints [8].

Upon conducting Cross-plot analysis, it is evident that the determination of the GR_THOR value at *XRD_Vcl* = 0% should be regarded as the exclusive GR Clean point for the T-Unit in the TAM field. Similarly, the GR_THOR value at *XRD_Vcl* = 100% is to be utilized as the GR Clay for the T-Unit in the TAM field. Consequently, to establish unique clean and clay points for Neutron and Density, it is imperative to employ the same approach by plotting the Neutron and Density logs against *XRD_Vcl* (Fig. 11).

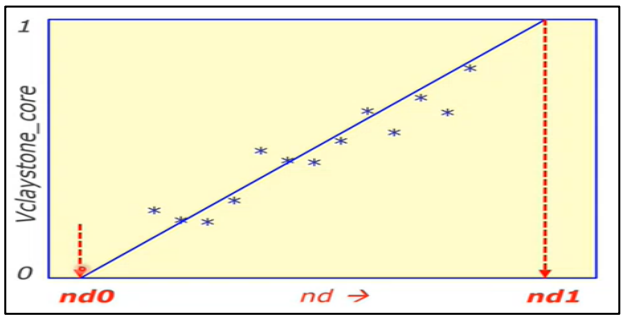


**Fig .11.** Ideal representation of N-D vs XRD_Vcl Cross plot for determining endpoints[8].

## 2.3 Data Gathering, Validation and Preliminary Results.

In conducting the *Log_Vcl* calibrations, we specifically chose to focus on the four systematically sampled wells. This selection included two wells from the Northern section and two from the Southern section of the TAM field. After carefully scrutinizing the XRD data, we noted that the *Log_Vcl* readings were notably higher in comparison to the *XRD_Vcl* analyses. Referring to Track 5 of Fig. 12, it is evident that the *Log_Vcl* value for well 9L06 surpasses the corresponding *XRD_Vcl* value. In addition, an elevated GR reading was observed in T3 Sand, while the *XRD_Vcl* analysis indicated a lower *Vcl* content.

In Fig.13, the VCLND displays similarly low *Vcl* values compared to the VCLGR. The X-ray diffraction (XRD) analysis revealed high concentrations of K-feldspar in the designated zones. It is crucial to emphasize that relying on the GRKT curve for estimating clay volumes in reservoirs may lead to inaccurate results in areas where non-clay minerals, such as K-feldspar, influence potassium-rich reservoirs. This discrepancy can result in an overestimation of clay volumes within the designated zones, as illustrated in Figures 12 and 13. In response to this issue, the GR_THOR method has been employed as an alternative approach to calculate clay volumes within identified potassium-rich reservoirs.

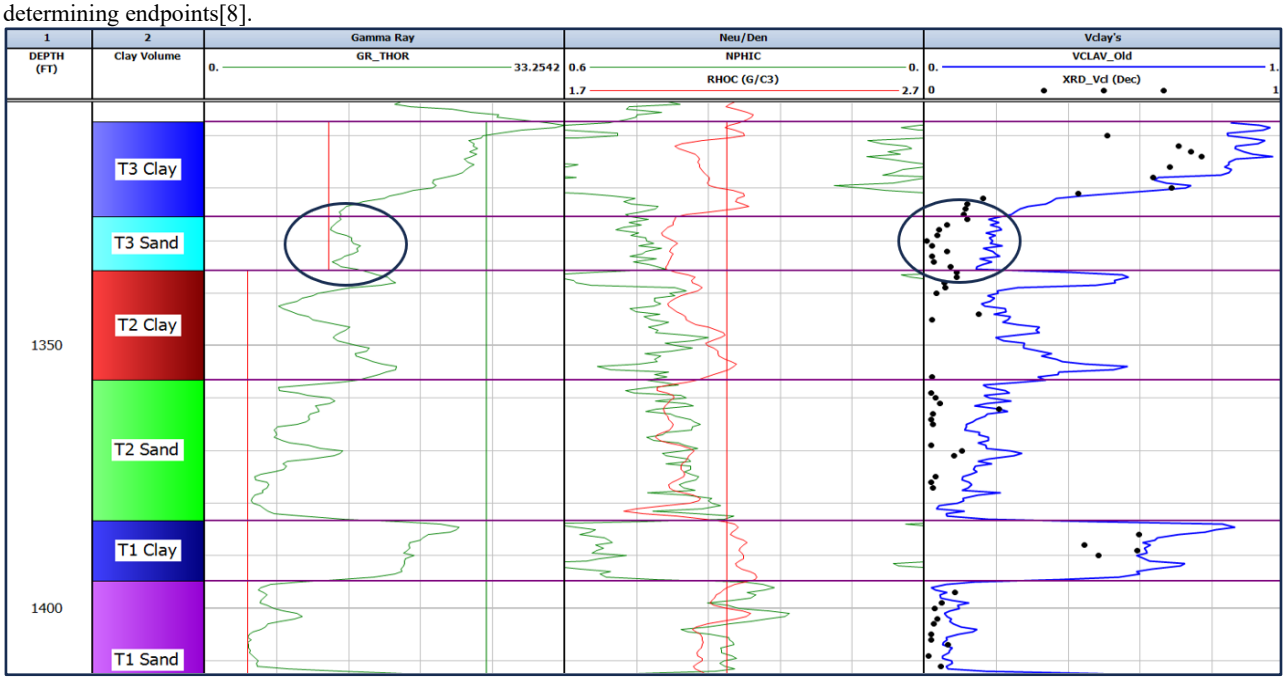


**Fig. 12.** Track 5 Shows that Log_Vcl (blue curve) is overestimated compared to XRD_Vcl.

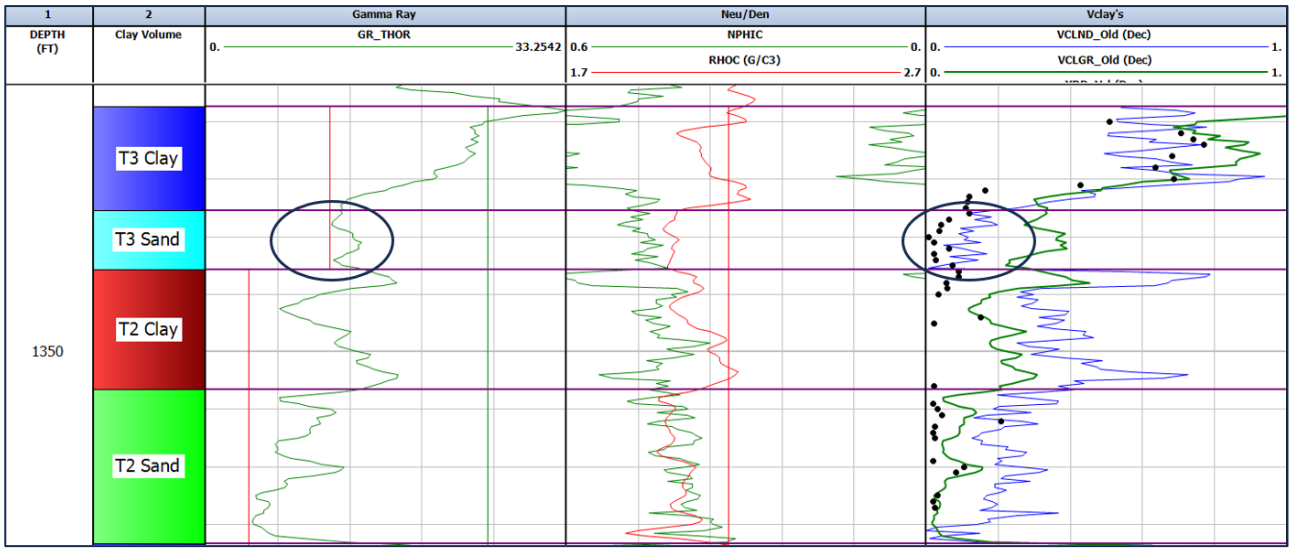


**Fig. 13.** VCLGR values are higher than XRD_Vcl while VCLND values are closer to the XRD_Vcl for T3 Sand.

## 2.4 Unique endpoint determination from log to XRD calibrations

In Fig.14, we observe the GR_THOR vs *XRD Vcl* cross plot, which was employed to identify the distinctive GR_Clean and GR_Clay endpoints for the T unit in the TAM field. The data used to construct the aforementioned plot was sourced from four selected wells – 30HM111, 1M101, 9L06, and 9B111 featuring XRD data. However, divergent trends were noted on the plot, which presented challenges in determining clear endpoints. As a result, the data was segregated into two sets: one set comprising the wells from Tambaredjo North (TAMN) (9L06 & 9B111), and the other set comprising the wells from Tambaredjo Central and South (TAMC & TAMS) (30HM111 & 1M101) in the TAM field.

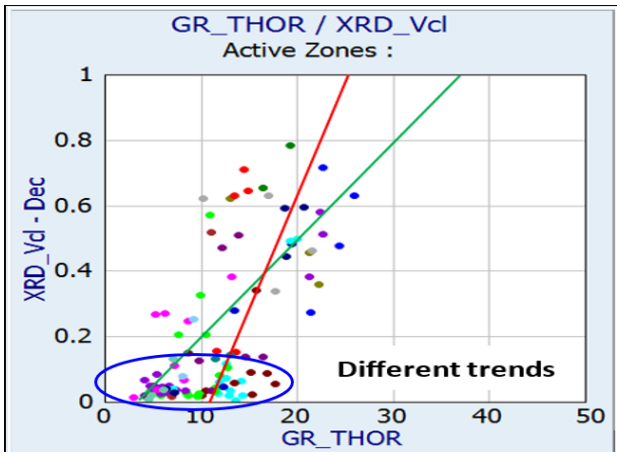


**Fig. 14.** GR _THOR vs XRD_ $V_{cl}$ to determine unique clean and clay points for the T-Unit in the TAM field.

Fig. 15 illustrates the relationship between GR_THOR and *XRD_Vcl* in a cross plot for the TAMC and TAMS wells (30HM111 & 1M101). The trendline observed in the plot implies that the clean value for GR_THOR should be approximately 4 parts per million (ppm).

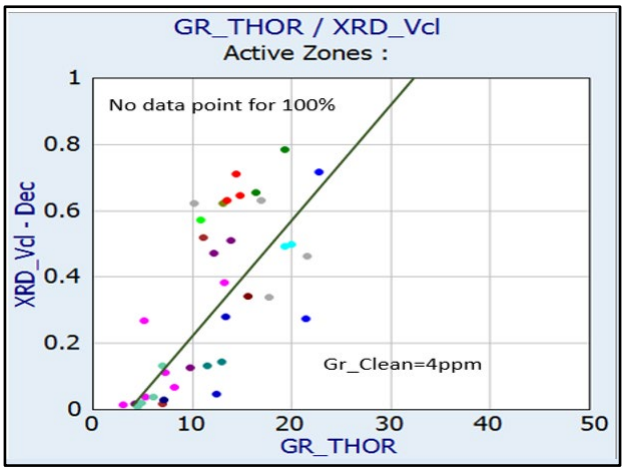


**Fig. 15.** GR _THOR vs XRD_ $V_{cl}$ to determine uniform clean and clay points, for wells in TAMC & TAMS.

The same approach was applied to the wells in *TAMN* (9L06 & 9B111) revealing, different trends for the *GR_Clean.* (Fig. 16).

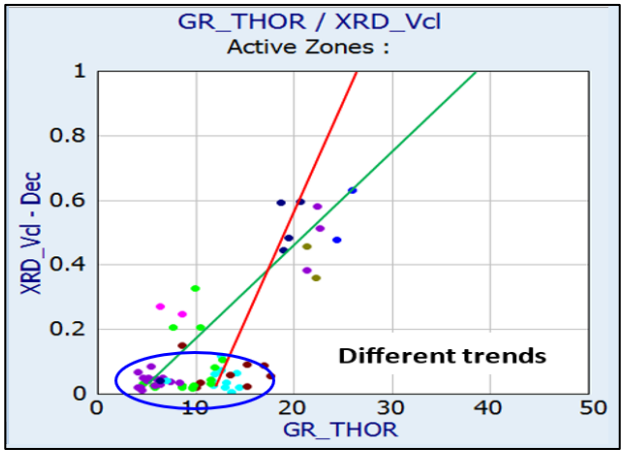


**Fig. 16.** Due to the presence of high K-felspar different trends are observed when plotting GR _THOR vs XRD_ $V_{cl}$ for TAMN area.

Upon dividing the TAMN area into the T3 and the (T2 & T1) Units, distinct GR_Clean points were identified. It can be inferred that the T3 unit exhibited a varying GR_Clean in the northern part of the field, likely attributed to its distinct depositional environment in comparison to the T2 & T1 units (Fig. 17 & 18).

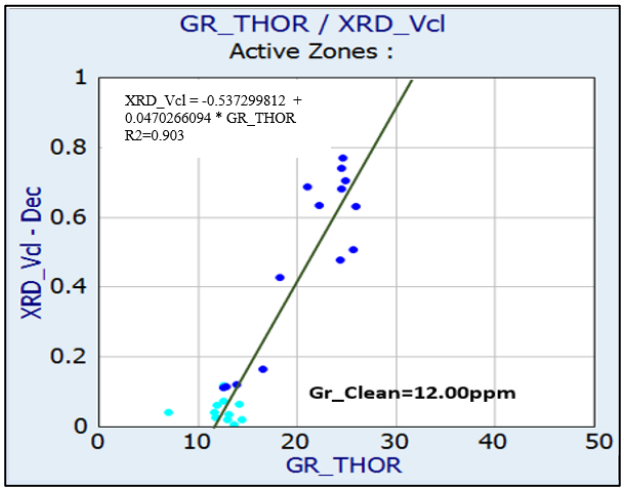


**Fig. 17.** GR _THOR vs XRD_ $V_{cl}$ cross plot for the T3 unit in TAMN. Determines a unique clean point for the T3 unit which is in a felspar-rich environment.

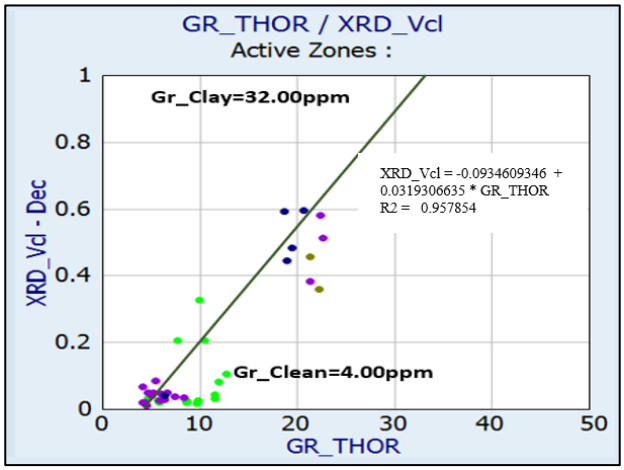


**Fig. 18.** GR _THOR vs XRD_ $V_{cl}$ cross plot for the T2 & T1 unit in TAMN. A separate Unique clean point was determined.

*for these units. By using an extrapolation method also a unique clay point could be determined*

The lack of *XRD* data containing 100% clay prevented us from determining a *GR_Clay* point from the existing dataset. Therefore, an alternative extrapolation method was used to determine the clay point from the available XRD data for the clay zones.

## 2.5 Extrapolating Clay point from XRD and log data

The maximum clay content was extrapolated to estimate the clay point using the XRD data. The formula used was as follows:

$$\textbf{100\% Clay} = (\,1 / \text{XRD\_}V_{cl}\,) * \text{GR\_THOR} \qquad (5)$$

where only XRD data with XRD_$V_{cl}$ > 50% were used. Fig. 19 shows the following values, at a depth of 1320', the XRD_$V_{cl}$ = 0.69%, and the GR_THOR is 21.1ppm. Indicated data was used to estimate what the GR_THOR value should be for:

100% clay: (1/0.69) * 21.1= 30ppm.

Pointed out step was repeated for all XRD data with *XRD_Vcl* content greater than 50%. An average of these outcomes was chosen as the GR_THOR at 100% *Vcl*. The abovementioned approach was used to determine separate clay points for TAMN and for (TAMC&TAMS) wells. Also, a distinction was made in deciding clay points for the T3 unit and (T2 + T1) unit in both TAMN and (TAMC+TAMS)

A similar approach was used to determine the Clean and Clay points for the N and D curves. Fig. 20 shows a cross plot for Neutron vs XRD_*Vcl*, with derived NPHIC_Clay and NPHIC_Clean. Again, distinguishment was made between TAMN and (TAMC & TAMS) Also distinguishment was made between the T3 unit and the (T2 & T1 unit)

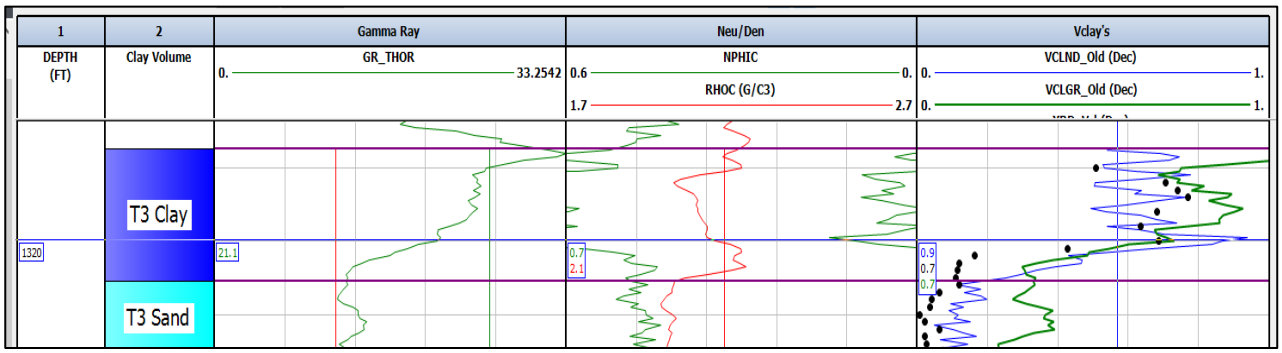


**Fig. 19.** GR_THOR and XRD_ $V_{cl}$ at depth 1320'used to extrapolate GR_THOR at $V_{cl}$ of 100%.

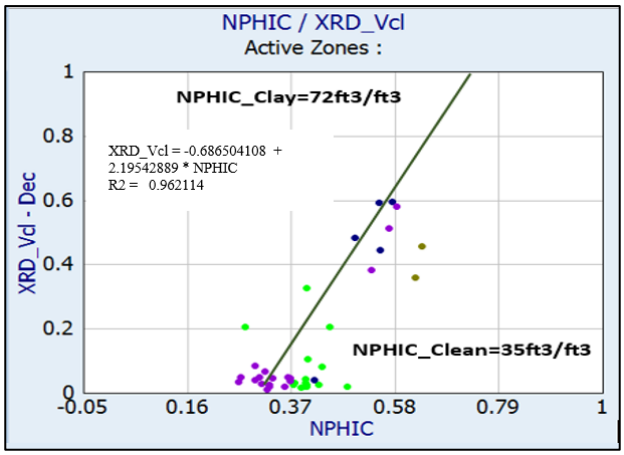


**Fig. 20.** NPHIC vs XRD_ $V_{cl}$ relationship for TAMN wells 9L06 & 9B111 for the (T1 & T2 Unit).

## 2.6 Creating a cross plot with shale triangle lines

An alternative method for identifying unique Neutron and Density clean and clay points involves creating a cross plot with shale triangle lines, as shown in Fig 21. This requires converting dry shale density from X-ray diffraction (XRD) to dry clay and then to wet clay. The resulting densities are averaged to produce the cross plot with shale triangle lines.

Additionally, a clear distinction is made between TAMN and (TAMC & TAMS).

**Table 1**. Determining wet clay density by converting dry shale to dry clay density to wet clay density from XRD data

From XRD data the ***dry shale density*** could be determined by summing up the density of the shale minerals.

| Depth Shift | XRD Composition | | Density gr/cc | Density per mineral vol. gr/cc | Dry Shale Density gr/cc |
|---|---|---|---|---|---|
| ft | mineral | vol. % | | | |
| 1310 | quartz | 32 | 2.648 | 0.85 | 2.72 |
| | k-feldspar | 7 | 2.554 | 0.18 | |
| | illite/mica | 1 | 2.85 | 0.03 | |
| | gypsum | 0 | 2.32 | 0.00 | |
| | calcite | 0 | 2.745 | 0.00 | |
| | dolomite (Fe) | 3 | 2.84 | 0.09 | |
| | siderate | 0 | 3.944 | 0.00 | |
| | marcasite | 0 | 4.75 | 0.00 | |
| | pyrite | 3 | 5.05 | 0.15 | |
| | illite/smectite | 6 | 2.608 | 0.16 | |
| | kaolinite | 46 | 2.65 | 1.22 | |
| | Chlorite | 1 | 2.95 | 0.03 | |
| | Plagioclase | 1 | 2.68 | 0.03 | |

The dry shale density was converted to ***Wet Clay stone density*** subtracting the total porosity and excluding the density from heavy minerals.

| Claystone | | Claystone (no heavy mineral.) | |
|---|---|---|---|
| Wet density | | dry den. | Wet density |
| gr/cc | vol. fract. normal | gr/cc | gr/cc |
| 2.35 | 0.35 | 0.92 | 2.67 | 2.32 |
| | 0.08 | 0.19 | |
| | 0.01 | 0.03 | |
| | 0.00 | 0.00 | |
| | 0.07 | 0.17 | |
| | 0.50 | 1.33 | |
| | 0.01 | 0.03 | |

***Wet Clay stone density*** was converted to **wet clay density** subtracting quarts and k-feldspar and then converted to ***wet clay density@ reservoir conditions.***

| Clay | | | Clay |
|---|---|---|---|
| | dry den. | Wet density | wet density |
| vol. fract. normal | gr/cc | gr/cc | reservoir conditions gr/cc |
| 0.113 | 0.295 | 2.65 | 2.30 | 2.15 |
| 0.868 | 2.300 | | |
| 0.019 | 0.056 | | |

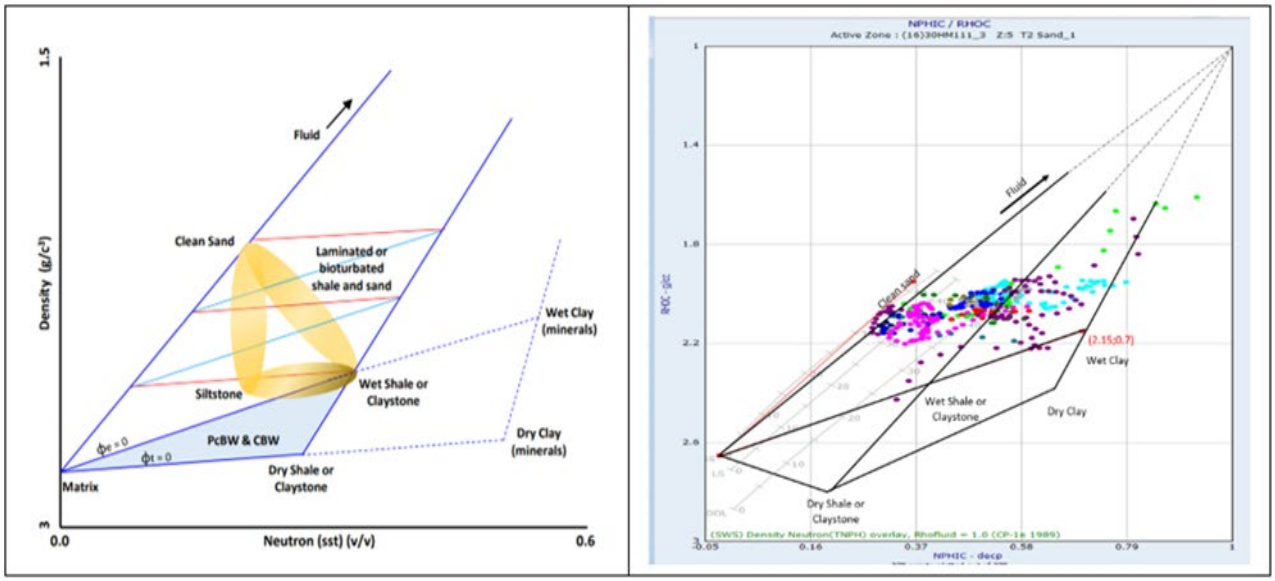


**Fig. 21.** Theoretical Cross plot with shale triangle line[9] vs cross plot with shale triangle lines as created for the T unit.

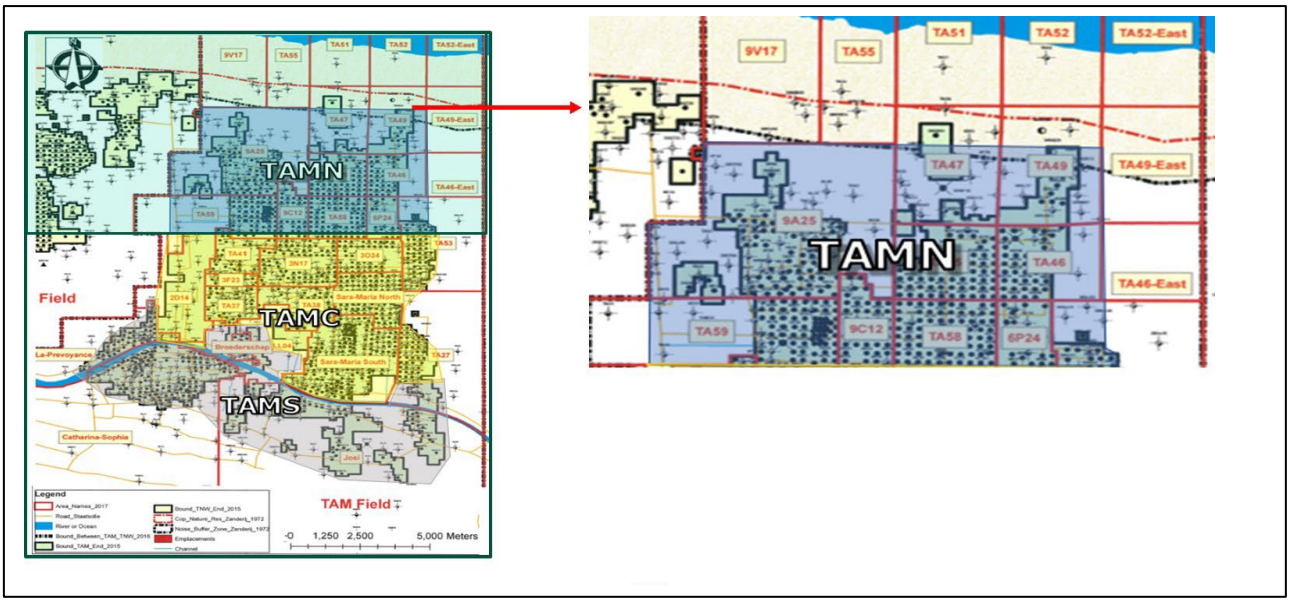


**Fig. 22.** Map of the TAM field divided in TAMN and (TAMC & TAMS) based on the derived unique Clean and Clay points[11].

**Table 2**. overview of the derived Unique Clay and Clean points for TAMN and (TAMC & TAMS).

**Ferhaad Idoe:**
For K environment

| Unique End points for wells with spectral logs in TAMN (reference wells 9L06 & 9B1110) | | | | | | | | |
|---|---|---|---|---|---|---|---|---|
| | GR_THOR_Clean | GR_THOR_Clay | NPHIC_Clay | NPHIC_Clean | | RHOC_Clay | | RHOC_Clean |
| | Gr Clean | Gr Clay | ND Neu Clay | ND Neu Clean 2 | ND Neu Clean1 | ND Den Clay | ND Den Clean 1 | ND Den Clean 2 |
| T3 Unit | 12 ± 2 | 28 ± 2 | 0.75 ± 0.05 | 0.40 ± 0.05 | -0.01 | 2.15 ± 0.05 | 2.65 | 1.95 ± 0.05 |
| T3 Unit | 4 ± 2 | 30 ± 2 | 0.70 ± 0.05 | 0.35 ±0.05 | -0.01 | 2.20 ± 0.05 | 2.65 | 2.00 ± 0.05 |
| T2 +T1 Unit | 4 ± 2 | 30 ± 2 | 0.70 ± 0.05 | 0.35 ±0.05 | -0.01 | 2.20 ± 0.05 | 2.65 | 2.00 ± 0.05 |
| Cret | 4 ± 2 | 15 ± 2 | 0.50 ± 0.05 | 0.20 ±0.05 | -0.01 | 2.15 ± 0.05 | 2.65 | 2.15 ± 0.05 |

| Unique End points for wells with spectral logs in (TAMC & TAMS) (reference wells 30HM111 & 1M101 ) | | | | | | | | |
|---|---|---|---|---|---|---|---|---|
| | GR_THOR_Clean | GR_THOR_Clay | NPHIC_Clay | NPHIC_Clean | | RHOC_Clay | | RHOC_Clean |
| | Gr Clean | Gr Clay | ND Neu Clay | ND Neu Clean 2 | ND Neu Clean1 | ND Den Clay | ND Den Clean 1 | ND Den Clean 2 |
| T2+T3 Unit | 4 ± 2 | 27 ± 2 | 0.70 ± 0.05 | 0.35 ±0.05 | -0.01 | 2.15 ± 0.05 | 2.65 | 1.95 ± 0.05 |
| T2+T1 Unit | 4 ± 2 | 18 ± 2 | 0.70 ± 0.05 | 0.35 ±0.05 | -0.01 | 2.15 ± 0.05 | 2.65 | 1.95 ± 0.05 |
| Cret | 4 ± 2 | 15 ± 2 | 0.50 ± 0.05 | 0.28 ±0.05 | -0.01 | 2.15 ± 0.05 | 2.65 | 2.10 ± 0.05 |

| Unique End points for wells without spectral logs | | | | | | | | |
|---|---|---|---|---|---|---|---|---|
| | GR_THOR_Clean | GR_THOR_Clay | NPHIC_Clay | NPHIC_Clean | | RHOC_Clay | | RHOC_Clean |
| | Gr Clean | Gr Clay | ND Neu Clay | ND Neu Clean 2 | ND Neu Clean1 | ND Den Clay | ND Den Clean 1 | ND Den Clean 2 |
| T2+T3 Unit | 4 ± 2 | 27 ± 2 | 0.70 ± 0.05 | 0.35 ±0.05 | -0.01 | 2.15 ± 0.05 | 2.65 | 1.95 ± 0.05 |
| T2+T1 Unit | 4 ± 2 | 18 ± 2 | 0.70 ± 0.05 | 0.35 ±0.05 | -0.01 | 2.15 ± 0.05 | 2.65 | 1.95 ± 0.05 |
| Cret | 4 ± 2 | 15 ± 2 | 0.50 ± 0.05 | 0.28 ±0.05 | -0.01 | 2.15 ± 0.05 | 2.65 | 2.10 ± 0.05 |

# 3 Results:

## 3.1 Division of TAM field in Area 1 (TAMN) and Area 2 (TAMC & TAMS).

Based on the analysis of the endpoints represented in the cross plots provided, it can be deduced that the TAM field can be partitioned into two distinct areas, as illustrated in Fig. 22 this division also corresponds with the depositional environment of the reservoirs:

- Area 1: Relates to the TAMN deltaic environment.
- Area 2:Reflects the TAMC & TAMS fluvial environment.

Table 2 presents all the unique endpoints identified for the TAM field, distinguishing wells from TAMN and (TAMC & TAMS) also between the T3 Unit in felspar-rich environment and non-felspar-rich environment and the (T2 & T1) unit.

In Fig. 23 the outcomes of VCLGR_THOR and VCLND are depicted after the application of the derived Unique endpoints. Upon assessing against *XRD_Vcl*, it can be deduced that VCLGR_THOR exhibits a superior alignment with the XRD data. Consequently, it is recommended to utilize the subsequent equation for the computation of VCLAV:

$$VCLAV = (06 * VCLGR) + (04 * VCLND) \quad (6)$$

In Fig. 24, a comparative analysis is presented between *XRD_Vcl*, the revised VCLAV, and the previous VCLAV. This examination illustrates that the revised VCLAV closely corresponds with the *XRD_Vcl*.

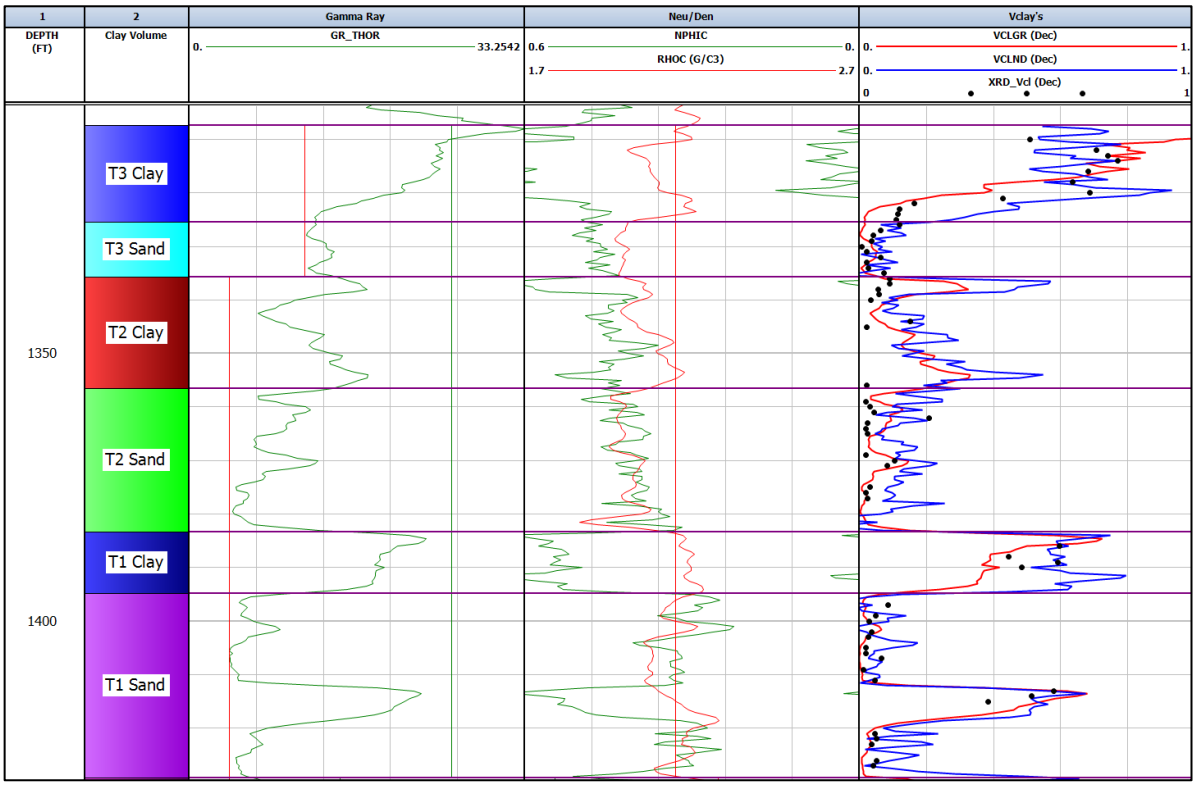


**Fig. 23.** XRD_Vcl, VCLGR and VCLND plotted in track 5 showing that both the VCLGR and VCLND matches the XRD_Vcl after the updates done to clay volume model.

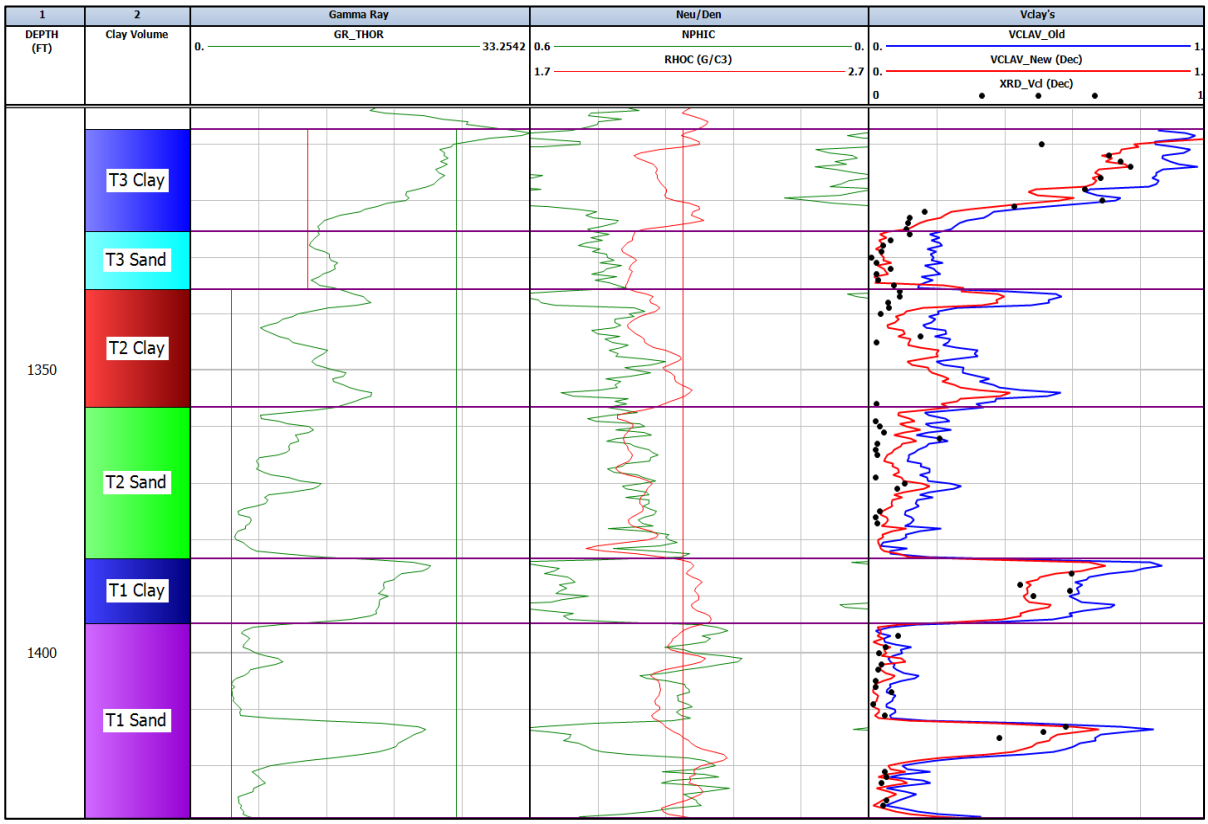


**Fig. 24.** XRD_Vcl, VCLAV_old and VCLAV_Updated plotted in track 5 showing that the VCLAV_Updated gives a better match with XRD_Vcl after the updates done to the clay volume model.

### 3.2 Results Diff Vclav_Old vs Vclav_Updated

The illustration in Fig. 25 depicts the variances in *Vcl* prior to and following the modifications made to the Clay volume using the revised model for the 3N17 area in the TAM field. It is evident across all three Units that the *Vcl* exhibits a decrease subsequent to the updates.

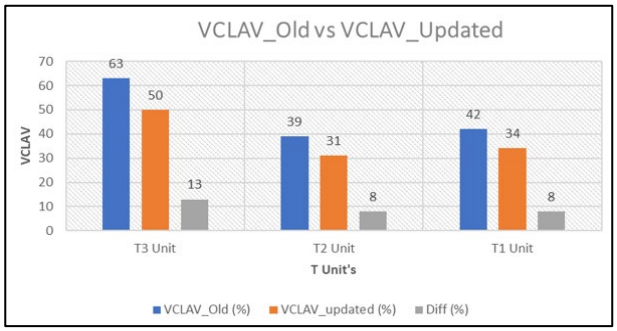


**Fig. 25.** VCLAV_Old vs VCLAV_Updated for the 3N17 area in the TAM field.

Fig. 26 depicts the contrast in *Sw* before and after the Sw equations were executed to account for the revised clay volume in the 3N17 area within the TAM field. It is evident across all three units that the *Sw* decreases as a result.

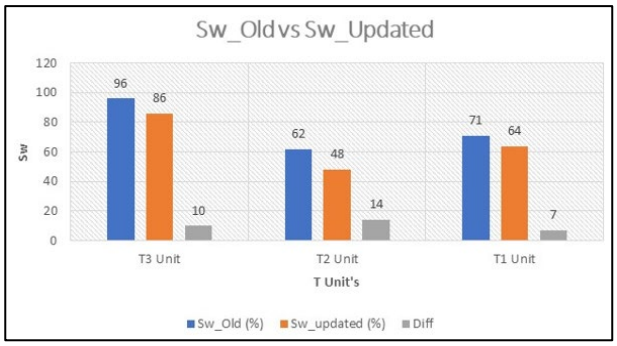


***Fig. 26*** *Sw_Old vs the Sw_Updated for the 3N17 area in the TAM field.*

## 4 Conclusions

- The Tambaredjo field was spatially segregated into two distinct regions, TAMN and (TAMC & TAMS), delineated by unique endpoints and depositional environments.
- It is important to note that the distinct sets of singular endpoints for TAMC and TAMS could be due to the influence of prevalent kaolinitic clays in these specific field areas.
- The endpoints for Area 1 and Area 2 were tested on nearby offset wells, and the results were mostly reliable with some minor adjustments.
- The distinct endpoints were obtained for wells within a K-feldspar-rich setting, which prevails in the T3 Unit in TAMN but may also sporadically occur in the T2 Unit.
- For wells lacking Spectral logs, the distinct endpoints are determined by utilizing the gamma ray (GR). Nonetheless, the *Log_Vcl* may still be overestimated due to the unresolved contributions of Uranium and K-feldspar.
- Upon adjusting the clay volume, the *Vcl* exhibited a decrease, leading to a reduction in Sw and a rise in PIIP.
- Distinct endpoints will provide the benefits outlined below in contrast to the drawbacks of individual endpoints.

**Table 3.** Advantages and disadvantages.

| | Advantages | Disadvantages |
|---|---|---|
| Log_Vcl derived from unique end points Callibrated with XRD data | Formation Evalaution done for Multiple wells simultaneously | |
| | Improved Clay volume | |
| | Improved PIIP | |
| | Avoid having the influence of different interpretars on the Vcl calculations | |
| Log_Vcl from individual end points without XRD callibration | | Formation Evaluation for individual wells |
| | | Overestimated Clay volume |
| | | Under estimation of PIIP |
| | | Different interpretars will use different end points resulting in differences in Vcl calcualtions |

## 5 Recommendations

- In order to guarantee optimal functionality, it is important to utilize separate endpoints for TAMN and (TAMC & TAMS).
- For the final *Log_Vcl* calculation, use an adjusted approach for VCLAV:

$$VCLAV = VCLAV = (06 * VCLGR) + (04 * VCLND)$$

- It is imperative to conduct a more systematic sample acquisition over depth in order to procure more dependable results for Log to Core calibrations.
- To attenuate the impacts of potassium feldspar, it is advisable to employ the GR_THOR curve instead of the GRKT for *Log_Vcl* calculations.
- Propose an additional project to be implemented utilizing artificial intelligence for the purpose of identifying radioactive minerals in wells lacking spectral logs.
- Identify the relationship between different clay types and *Sw*.

The authors would like to acknowledge, J. Oedietram (Sr. Petrophysicist), D. Ramesar (Sr. Petrophysicist) and A. Nelson (Manager FSS), for their comments and encouragement during this study. Additionally, we acknowledge the use of the Gemini AI chat (Google) as an aid to improve this article's English grammar and readability.

## Nomenclature

CAL = Calcutta
GR = Gamma ray
GRI = Gamma ray index
GRKT = Gamma ray Potassium Thorium
GR_THOR= Gamma ray Thorium
K-felspar = Potassium felspar

K = Permeability
Log_Vcl = log clay volume
N-D = Neutron-Density
PHIE = Effective porosity
PHIT = Total porosity
PIIP = Petroleum initially in place
SGR = Spectral Gamma Ray
Sw = Water Saturation
TAM = Tambaredjo
TAMC = Tambaredjo Central
TAMN = Tambaredjo North
TAMS = Tambaredjo South
TNW = Tambaredjo North West
Th = Thorium
Vcl = Clay volume
VCLAV = Average clay volume
VCLGR = Gamma ray clay volume
VCLND = Neutron-Density clay volume
XRD = X-ray diffraction
XRD_Vcl = X-ray diffraction clay volume

## References


1. S. Toelsi, Impact of Depositional Environment on Vertical Reservoir Sand Distribution, Anton de Kom University of Suriname, (2013).
2. F. Stapor, *Sedimentologic and Stratigraphic Model of the T-Unit, Saramacca Formation (Paleocene), Tambaredjo Field -EOR Gas Project,* MK Tech Solutions. (2013).
3. Core Laboratories, Inc., *Sedimentology and Petrology Well 9B11-1 Tambaredjo Field Suriname, Houston, Texas,* (2007).
4. J. Tourne, *Suriname Petrophysical and Reservoir Analysis from Core and Logs Integration, Sarah Maria, Suriname,* JPT Consulting and Services, (2008).
5. PanTerra GeoConsultants B.V., *Tambaredjo RCS for the Polymer Flood Expansion Area – Petrophysical Evaluation,* PanTerra, (2014).
6. P. Naigi, *Calibration of Clay Volume with XRD Data in the TNW Field,* Staatsolie Maatschappij Suriname N.V., (2017).
7. A. Lieveld, *Calibration of the Clay Volume Method for Staatsolie Paleocene Reservoirs using X-Ray Diffraction Data,* Antom de Kom University of Suriname, (2019).
8. M. Deakin, *Review of Clay Volume Data, Method and Calculations Tambaredjo Field, Suriname,* Petrophysics Pty Ltd, (2022).
9. R. Aldred**,** *Review of the Volume of Clay Calculations in the Tambaredjo Field,* R. A. Petrophysical Consulting, (2022).
10. Geoactive Ltd, *Interactive Petrophysics Help Module,* (2024).
11. E. Acosta, *PETROPHYSICS Standardization Handbook, Guidelines for the updated Water Saturation Model (phase I) for Tambaredjo Paleocene Reservoirs,* Staatsolie Maatschappij Suriname N.V., (2022).